International Journal of Disaster Risk Reduction 111 (2024) 104758

Contents lists available at ScienceDirect

International Journal of Disaster Risk Reduction

journal homepage: www.elsevier.com/locate/ijdrr

Flood scenario spatio-temporal mapping via hydrological and hydrodynamic modelling and a remote sensing dataset: A case study of the Basento river (Southern Italy)

Raffaele Albano [a,*], Carmine Limongi [a], Silvano Fortunato Dal Sasso [b], Leonardo Mancusi [c], Jan Adamowski [d]

[a] School of Engineering (SI), University of Basilicata, Potenza, Italy
[b] Department of European and Mediterranean Cultures (DICEM), University of Basilicata, Matera, Italy
[c] Department of Sustainable Development and Energy Sources, Research of Energy System (RSE S.p.A.), Milano, Italy
[d] Department of Bioresource Engineering, McGill University, Sainte-Anne-de-Bellevue, QC, Canada

ARTICLE INFO

Keywords:
Model calibration
Hydrodynamic modelling
Hydrological modelling
SAR
Flood mapping

ABSTRACT

Today, hydrological and hydraulic modelling are essential tools for flood risk management, although these models are still affected by elements of uncertainty that needs to be reduced by optimizing their results. The present research aims to implement an operational mechanism on the Basento river basin in Southern Italy based on the cascading use of a physically based concentrated-parameter hydrological model for the estimation of flood hydrographs, and a two-dimensional hydraulic model for flood mapping. The calibration of the hydrological model uses physical information to reduce the initial range of the set parameter values, and an automated optimisation procedure based on a genetic algorithm to find optimal values of the model parameters by comparing simulated and observed data for the 2013 flood event. To calibrate the hydraulic model, a series of flood maps extracted from multi-temporal SAR images was used. In addition, validation of the hydrological and hydraulic models was carried out on March 2011 flood event. The results show the reliability of the models during both calibration and validation, with the hydrological model achieving a Nash-Sutcliffe Efficiency coefficient between 0.86 and 0.91, and the hydraulic model leading to results with an accuracy close to 70 %. Considering the significance of the results, the developed modelling chain was used to simulate future event scenarios for risk management assessment and could operate as an early warning system.

1. Introduction

One-third of the economic losses due to natural hazards in Europe are related to flooding and it is one of the most frequent hazards [1]. The identification of flood hazards and risk scenarios as well as short-term forecasting of flood events and the potential impact of floods on portfolios of assets is of primary interest to various stakeholders, such as property owners, (re)insurance companies, and local government agencies, among others [2].

Flood scenario mapping is an essential tool in integrated flood risk management, as numerous management strategies depend on understanding the inundation probabilities of different areas [3]. These maps provide valuable quantitative estimates of flood hazards

* Corresponding author.
E-mail address: raffaele.albano@unibas.it (R. Albano).

https://doi.org/10.1016/j.ijdrr.2024.104758
Received 27 May 2024; Received in revised form 11 August 2024; Accepted 12 August 2024
Available online 13 August 2024

that stakeholders can utilize for a range of purposes, such as designing structural defences like levees and retention basins, which must be tailored to specific probabilities (*e.g.*, a 1 % annual exceedance probability or a 100-year return period), or to planning non-structural measures such as evacuation plans and insurance policies [4]. Hence, accurate flood scenarios estimates, along with an understanding of their uncertainties, are fundamental to effective risk adaptation and the development of appropriate design variables in engineering solutions.

To achieve a comprehensive assessment of flood risk, it is crucial to combine hazard estimates (revealing the frequency, intensity, and distribution of floods) with vulnerability models. These models assess factors like population density, socio-economic conditions, and infrastructure resilience, providing a comprehensive view of potential impacts. Integrating hazard and vulnerability data enhances risk accuracy and supports targeted mitigation strategies, such as improved drainage systems and community awareness programs, ultimately helping to design effective disaster preparedness and resilience measures.

In particular, hazard hydrodynamic variables, such as water depth and flow velocity, can be computed typically by using hydrological models, for discharges estimation, coupled with hydraulic models, for flood propagation simulations, which represent a well-established approach for flood risk analysis. In recent years, hydrological/hydrodynamic modelling of flood events has seen exponential improvements, thanks to the development of increasingly reliable and efficient numerical methods, increased computing power and innovative geomatic techniques. Recent technological developments have favoured the use of 2-D flood simulations, replacing 1-D approaches which, despite their efficiency and ability to reproduce processes within a channel, present conceptual problems when the typical flooding of urban environments occurs [5]. Flood hazard maps derived from this physically based modelling should provide substantial information on the extent of a possible flood with a given frequency, and on the distribution in terms of space and time of water depth and flow velocities. However, it is important to consider the validity of assumptions inherent in the map generation method and the inevitable uncertainties present in the forecasting process for proper use of such maps in decision-making processes. Some of these uncertainties can be reduced by using accurate high-resolution topographic data [6,7], historical data collected in-situ or via satellite to better parameterise the models [8–11], and also by using intensive calibration procedures to find the optimal set of parameters [12]. Therefore, the goal should always be an optimal balance between detail, abundance of input data and complexity of the model, chosen based on the objective of the study and the application.

In recent decades, remotely-sensing techniques, such as airborne photogrammetry, space-borne Interferometric Synthetic Aperture Radar (InSAR) and Light Detection and Ranging (LiDAR) have allowed the creation of Digital Elevation Models (DEMs) at a global scale (*e.g.,* NASA's Shuttle Radar Topography Mission, SRTM). High-resolution satellite imagery (*e.g.*, Sentinel-1, Sentinel-2, and Landsat 8) are used for detecting and extracting flood-affected areas although satellite tracking may not always coincide with cloud-free conditions or flood peaks related to the maximum inundation area. SAR data combined with a DEM are considered very useful sources of information to extract water depth maps in a flat terrain with complex topography [13]. For instance, the Copernicus Emergency Management Service ([14]; https://emergency.copernicus.eu/) uses optical and/or Synthetic Aperture Radar (SAR) data based on their availability to provide timely and accurate information for emergency response and disaster risk management. Indeed, the increasing availability of spatio-temporal data has overcome some limitations related to data scarce environments, facilitating a spatial pattern-oriented model calibration and validation[15]. In recent years, several sources of remotely-sensed information such as evapotranspiration, surface soil moisture, and Nor malized Difference Vegetation Index (NDVI) were used in order to incorporate this spatio-temporal information during the calibration process, using multi-criteria approaches.

According with Flood Directive (2007/60/CE) that recommends the use of the most advanced models for the assessment of flood prone areas, this research lies in the development and application of a new comprehensive approach for flood hazard assessment. The proposed approach, has been tested to: 1) analyse and reconstruct the past flood events in Basento basin in Basilicata (Italy); 2) to evaluate flood event scenario maps with given return times and their spatio-temporal evolution at the Basento mouth, where several calamitous floods have caused severe damage.

The core of the framework involves combining a hydrological model with a hydraulic model, appropriately calibrated and validated using time-series and spatially distributed data from past events. More specifically, it includes the cascading use of a physically-based, concentrated-parameter inflow-outflow hydrological model to estimate flood hydrographs and a two-dimensional hydraulic model to calculate hydraulic characteristics such as flood extent and maximum envelope of water depth. The overall conceptualisation of the workflow of the mapping has been based on previous studies (*e.g.* Ref. [16]) but with a greater emphasis on the ingestion and combination of heterogeneous data from different sources considering the application in a data-scarce environment and reduction of the different source of uncertainty, *e.g.* estimation of flood discharge and hydrodynamic modelling, that can have a big effect on the accuracy of the resulting flood hazard maps. When less information is available, uncertainties are larger, but the proposed approach contributes to an overall strengthening of the outcomes.

The calibration and validation of these hydrological and hydrodynamic models allows us to identify optimal parameters for hazard assessments in the study area characterised by a complex topography (featuring embankments, banks, bridges, etc.). The models are expected to accurately determinate future event scenarios for given return times, and can also be used for short-term forecasting purposes. The hydrological model's calibration and validation process includes a genetic algorithm technique, which automatically makes subsequent trials of model parameters and makes use of numerical criteria to evaluate their goodness compared with observed measurements. In this way, it obtains an optimal set of parameters within a delimited range of the parametric space of variables. The use of a very large set of parameters can define a wide spectrum of possible solutions of the hydrological model. Therefore, to avoid unacceptable solutions from a physics perspective, the choice was made to use physical information, such as ground cover, soil texture or slope, to reduce the search range of the automatic algorithm in a physically-based range of parameter variation.

The calibration and validation of the hydrodynamic model are carried out using wetted area maps of previous major flood events derived from multitemporal SAR images [17], which considers the effects of channel roughness coefficients for channelled flow and

floodplain runoff (sheet flow). The decision to use a combination of SAR imagery and a genetic algorithm when calibrating the models is to enable us to produce timely and accurate outputs that best describe the expected scenarios.

2. Area of study

The case study is the Basento River basin, which originates in the northern Lucanian Apennines and flows from north-west to south-east in the provinces of Potenza and Matera into the Gulf of Taranto. The Basento River extends 149 km and is the longest river in Basilicata and the longest of the Italian rivers flowing into the Ionian Sea. The catchment area covers approximately 1535 km^2, with more than 70 % of the total surface covered by agricultural areas and the remainder characterised by coastal forests and vegetation typical of some Mediterranean areas. The northwest is mountainous, then becomes hilly and gradually degrades towards the coastal plain of the Metapontine area in the east. The entire basin has an average elevation of 613 m and an average slope of 15 %. Its mountainous part is characterised by marked topography, whereas its terminal portion, near the closure section, is extremely flat.

The aim of this study is to estimate the flood discharge hydrograph with given return times at the "SS 106 Jonica" cross-river section and to use these data for mapping flood event scenarios simulated by hydrodynamic models in a test area of approximately 124 km^2 that extends 7.5 km upstream from the mouth of the Basento River (Fig. 1). For the hydrological analysis, this study focused on the part of the Basento that extends upstream of the hydrometric station called "Basento SS 106", close to SS 106 Jonica Road, where the flood hydrograph was reconstructed (i.e. the evolution of the flow rate over time). For the hydraulic analysis, the area examined stretches from the "Basento SS 106" station to the river mouth, close to the sea, where the assessment of the floodable areas was carried out. This study area was selected due to the concentration of several flooding phenomena in previous years, as reported by Manfreda et al. [18], in an analysis of the main floods that occurred in the Basilicata from 1921 to 2014, placing the entire area among the most at-risk.

Of particular relevance are two flooding events that affected the Basento River and occurred between 1 and March 2, 2011 and between 2 and December 3, 2013 causing extensive damage. The March 2011 event was particularly severe due to the intense rainfall in the hinterland of Matera, where the highest concentration of precipitation was recorded; a total of 139 mm measured between 1:00 a.m. and 9:00 p.m. on 1 March at the Ferrandina weather station [39]. The rainfall event of December 2013 began in the late afternoon of November 30, 2013 and ended in the evening of December 3, 2013, with the maximum rainfall occurring on 1–2 December, affecting the regional territory with values that locally exceeded 150 mm for the entire event (*e.g.*, at the "Basento freatimetro" station - see Fig. 2) [40].

3. Materials and methods

3.1. Dataset Description

Precipitation (i [mm/h]) and discharge (Q [mc/s])] data from the monitoring networks managed by the Basilicata Region for the events of March 2011 and December 2013 were collected and catalogued at hourly intervals. In particular, discharges were obtained using hydrometric stage measurements at the "Basento SS 106" station and the flow-rating curve from Bancheri et al. [19]. For rainfall input, data from 20 weather stations, considered representative of the area, were identified and analysed. The Thiessen polygon method [20], based on simple geometric considerations, was used to determine the areas pertaining to each pluviometric station. Fig. 2 shows the pluviometric stations used for hydrological modelling and the Thiessen polygons obtained.

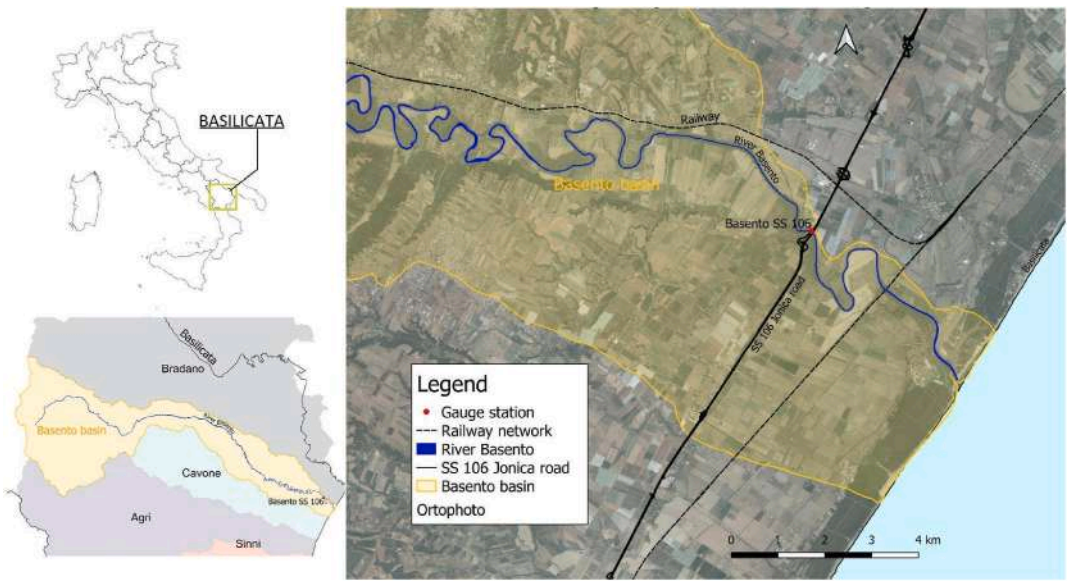

Fig. 1. Case study placement.

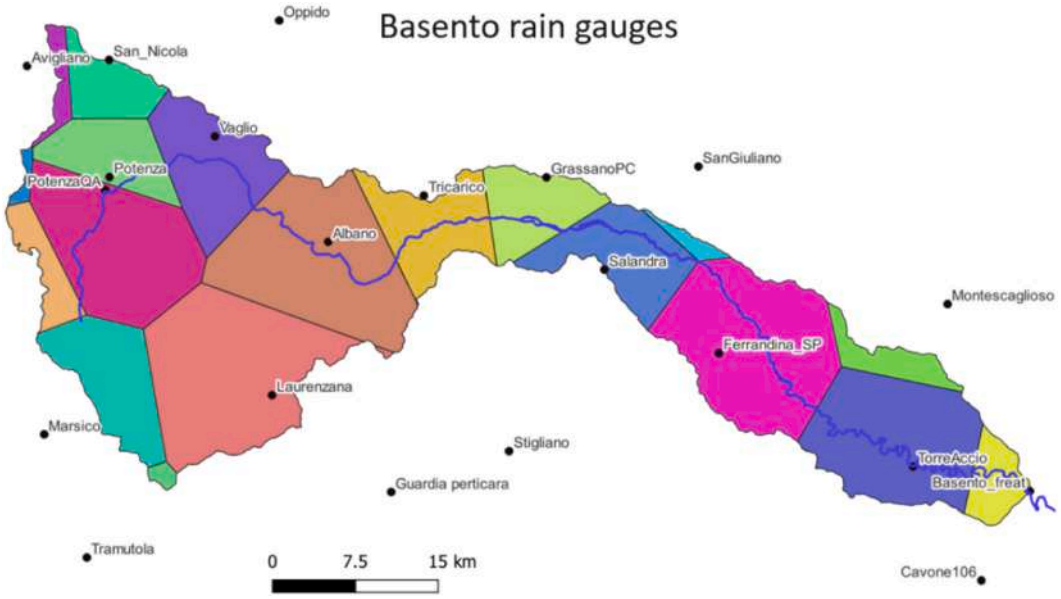

Fig. 2. Rain gauge locations and related Thiessen polygons in the basin upstream of the cross section "Basento SS 106".

In addition, multi-temporal Cosmo-SkyMed SAR images for these two flooding events (Single-look Complex Slant SLC Products), executed in Stripmap mode with a resolution of 2.5 m and featuring horizontal or vertical polarisation, were used to estimate the wetted flood areas during the above-mentioned events [13]. For each event, one of the SAR images was captured a few weeks before the event, while the others were captured during the event. For the 2013 event, one image is available specifically in the phase preceding the flood peak (on the ascending branch of the flood hydrograph) and one immediately following the flood peak (in the descending phase of the flood hydrograph). For the 2011 event, only one image is available during the flood, and it is temporally positioned in the descending phase of the hydrograph.

The reconstruction of the hydro-pluviometric and remote-sensing dataset made it possible to identify the best values of the hydrological and hydraulic model parameters and their adaptation to the study context for the 2013 event, improving the modelling performance. Moreover, the validation assessment of the proposed methodology under different operating conditions has been performed over the 2011 event. Through calibration and validation, it was then possible to support the definition of spatio-temporal dynamic of future flood scenarios by limiting any uncertainties.

3.2. Methodology

The AD2 hydrological model [12] and the FLORA-2D hydraulic model [21] were used to outline hydraulic hazard maps for flood event scenarios with return times of 30, 200 and 500 years. The former is of the concentrated-parameter and physically-based conceptual type, capable of interpreting and describing hydrological process at the event scale. It was used to estimate the initial conditions (*i.e.,* the flood hydrograph) of the flooding scenarios simulated with the FLORA-2D two-dimensional model. The latter is based on De Saint-Venant's shallow water equations [22] and is suitable for simulating flood propagation in flat and mouth areas with complex topography.

A calibration and validation phase of these models, obtained by simulating the most significant flood events that affected the Basento, is essential to optimise the performance of the models, both in assessing event scenarios (here, for the three return times (T_R) of 30, 200 and 500 years) and in supporting flood forecasting and monitoring.

The overall methodology, schematised in Fig. 3, is composed of three main steps.

STEP 1 During the calibration of the AD2 model, the value variation range of the model parameters is initially defined by means of an analysis based on the morphological and geometric features of the basin. Subsequently, the value ranges, based on previous estimates, are optimised by adapting them to the flow measurements observed during the December 2013 event in the "Basento SS 106" section of the basin, using a genetic algorithm. In this specific case, the calibration is carried out by constructing an objective function, which uses the NSE index, *i.e.*, Nash-Sutcliffe's Efficiency coefficient [23], here calculated by comparing the hydrograph observed at the "Basento SS 106" section with that calculated with the AD2 model. To strengthen the methodology proposed, the AD2 model is validated against a second historical event that took place in the same area between 1 and March 2, 2011. Obtaining a significantly high NSE result thus demonstrates the performance of the model and the goodness of the values used for its parameters.

STEP 2 After completing the calibration and validation phase of the hydrological model, the next step concerns the calibration and validation of the FLORA-2D hydraulic model to outline the extent of the floodable areas processed from multi-temporal SAR satellite images (as proposed by authors in Ref. [13]), during the two historical events of March 2011 and December 2013. The

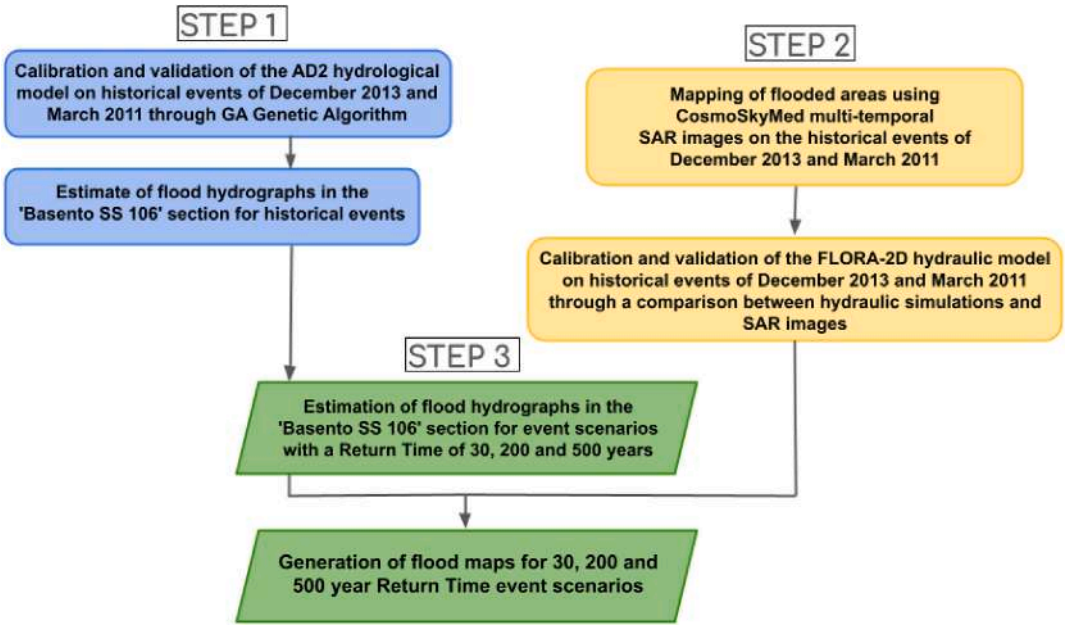

Fig. 3. Flow-chart of the overall methodology.

methodology used is based on a comparison between the flood maps extracted by SAR satellite images acquired before and after the peak phase of the event and the maps of the inundated areas generated by the FLORA-2D model for six different roughness values. From this comparison, the best values of the chosen parameter of the hydraulic model are analysed in order to adapt to the study context, optimizing the performance of the model and allowing the goodness (validation) of the proposed methodology to be assessed for multiple historical events.

STEP 3 Following the calibration and validation of the models using historical events, the next step is to evaluate both flood hydrographs and flood maps for the event scenarios with return times of 30, 200 and 500 years. In particular, the estimation of flood hydrographs by means of the AD2 model for the various event scenarios is carried out from rainfall for specific return times using the rainfall time series to estimate the pluviometric probability curves (PPCs), as indicated by Ippolito [24] for a duration equal to the basin's outflow time, and the regionalisation method VAPI Basilicata with subsequent updates as reported by Manfreda et al. [18] to extract it to high return times, and lastly, adopting the temporal precipitation distribution according to the Chicago method. Note that pluviometric probability curves express the relationship between precipitation height and duration over an assigned return period. To verify the representativeness of the hydrological model results for event scenarios, the return time of the December 2013 event, for which the hydrological model was calibrated, is first estimated. Then, the flood peak of this historical event is compared with that of the hydrograph obtained from the Chicago synthetic hyetograph with equal return time.

Since good results were obtained from this comparison, it was possible to use the methodology proposed above to define the flood hydrographs of events with $T_R = 30$, 200 and 500 years and to create maps of the distribution of water depth and current velocities using the hydrodynamic model FLORA-2D.

3.3. The AD2 inflow-outflow hydrological model

The AD2 hydrological model is a conceptual, event-scale, bucket model [25] in which surface outflow is generated by over-saturation [26] that exclusively considers the following components of the hydrological cycle: infiltration, surface run-off, sub-surface run-off, deep percolation. Interception and evapotranspiration due to vegetation are generally negligible during flood events. The hydrograph is generated as the sum of two variable contributions related to surface Q_s and sub-surface run-off Q_{sub} and a constant one called baseflow rate Q_b, which is equal to the flow rate value before the beginning of the flood event. The total flow rate is, therefore, evaluated as the sum of the three contributions.

The AD2 model requires as input a series of typical soil hydrology parameters, which can only be determined from an analysis of the basin itself. These parameters refer to physical processes or components and can be obtained partly through empirical formulations and partly through a geomorphological analysis of the basin. For example, parameters α_s and α_{sub} (Table 1) depend on the basin size or the other parameters which vary according to soil cover, soil class and slope. Other hydraulic parameters *Ks*, *n*, θ_c and β, necessary for the estimation of AD2 model parameters, depend on exclusive knowledge of the soil particle size classes.

Table 1 below schematises the hydrological parameters required by the AD2 model.

Table 1
AD2 model parameters.

N	Param.	Unit of measurement	Description
1	C	(−)	Surface run-off coefficient
2	S_c	(mm)	Water content at field capacity (mm)
3	S_{max}	(mm)	Soil storage capacity (mm)
4	c	(h^{-1})	Sub-surface flow velocity coefficient (l/h)
5	K_s	(mm/h)	Permeability at saturation (mm/h)
6	$c_{\_soil}$	(−)	Exponent of pore distribution in the soil
7	α_s	(h)	Surface run-off recession constant (l/h)
8	α_{sub}	(h)	Sub-surface run-off recession constant (l/h)

3.4. Calibration and validation of the AD2 inflow-outflow hydrological model for flood events in the Basento basin

During the calibration of the AD2 model, the value variation range of the possible model parameters was initially defined by means of an analysis based on the morphological and geometric features of the basin. Then, the optimal values that best fit the flow rate measurements observed during the December 2013 event in the section of the basin known as "Basento SS 106" were identified within the value ranges, based on the previous estimates, using a genetic algorithm (*e.g.,* Ref. [12]).

Genetic algorithms are tools that can be used to search for certain parameters by tentatively evaluating a large number of potential solutions. This approach generates several potential solutions, taking them from a search space according to the constraints set by the variation ranges. In fact, genetic algorithms are automated tools for calibrating models using an iterative parameter search. Each parameter class allows a new one to be generated from the previous conditions to produce gradually more efficient solutions by randomly searching for the optimal values of the parameters considered.

Operationally, an initial group of starting solutions is generated randomly (as if they were different individuals in a population) and from this group, new generations are created through combinations of the "best" individuals from the previous generation to which small random changes are also made (similarly to random genetic mutations). In our application, we set a population of 100 individuals and a maximum number of generations equal to 20. The measurement of how much a solution is better than another is based on a specially designed function called fitness function or objective function. In this specific case, the calibration was carried out by creating an objective function using the NSE index (Eqn 1), which allows the quantification of the consistency of a AD2 time series with in-situ measured one:

$$F(\theta) = 1 - \frac{\Sigma_{t=1}^{N} [Q(t) - \widehat{Q}(t)]^2}{\Sigma_{t=1}^{N} [Q(t) - \underline{Q}(t)]^2} \quad (1)$$

where $\underline{Q}(t)$ is the mean value of the observed discharge data registered at the "Basento SS 106" cross-section, $\widehat{Q}$ *(t)* the AD2 simulated discharge value at time *t* and *Q(t)* the observed value at time *t*.

The parameter values obtained in the calibration phase during the December 2013 event were then used to strengthen the methodology in the subsequent validation phase through the second historical event of March 2011.

3.5. Evaluation of flood hydrograph for the event scenarios with return times of 30, 200 and 500 years

The design hyetographs for the evaluation of peak discharges (*Qmax*) during flood events were derived from the Depth-Duration-Frequency (DDF) curve and the Intensity-Duration-Frequency (IDF) [27] for a duration equal to the basin's concentration time, adopting the time distribution of precipitation according to the Chicago method.

DDF curves express the relationship between precipitation height and duration over an assigned return period by a power law of the following type (Eqn 2):

$$h_{t,T} = K_T a t^n \quad (2)$$

where parameter *a* is expressed in mm and time t in hours; *a* and *n*, characteristic parameters of the rain gauge station, also depend on the specific return time assigned. To highlight the dependence of the precipitation value on return time *T*, the DDF takes *T* into account by introducing parameter K_T, known as the growth factor. The parameter is estimated as a function of the probability distribution by which a given phenomenon is studied.

In this case, parameters *a* and *n* and growth factor K_T derived from the TCEV distribution of observed data, contained in the report on the VAPI methodology in the Basilicata region [28] and subsequent updates [18], were adopted and the DDFs were calculated for each pluviometric station examined. Then, the rainfall event recorded for each pluviometric station considered was compared with these curves and the corresponding return time was determined. Given the return time of the recorded event and the law to determine the cumulative rainfall height (or intensity), the rainfall intensity trend over time for the duration of the project event (project hyetograph) was described. In this specific case, reference was made to the Chicago hyetograph with baseline time equal to the basin's concentration time.

To verify the consistency between the hydrological model calibrated on the December 2013 event and its application using the statistical hyetograph, the return time of that event was first estimated (equal to 19 years) and, then, the flood peak of the 2013 event was compared with that of the hydrograph obtained from the statistical hyetograph of equal return time.

Similarly, events with $T_R = 30$, 200 and 500 years were defined. The choice of return times was not accidental but dictated by the fact that these are used by district authorities in the Italian Flood Risk Management Plan [29].

3.6. Maps of floodable areas extracted by processing satellite SAR images

The methodology used to outline the extent of floodable areas processed from satellite images for a few time instants during the two historical events of March 2011 and December 2013, starts from the assumption that there is a high contrast between flooded and non-flooded areas in SAR satellite images [30]. Since the flooded areas are much more regular than the surrounding terrain and, therefore, reflect most of the radar signal, backscatter is very low and the flooded areas appear characterised by dark tones [31]. However, to avoid problems in identifying them, at least two Cosmo-SkyMed (CSK) images of the same area were used, before and during the event, to reduce the probability of classifying non-flooded cells as flooded, since shaded areas can be represented with dark pixels in the same way as flooded areas. This is why only pixels that significantly change their backscatter values between the two images are considered flooded areas. Specifically, the methodology involves three stages [13].

1. A threshold is identified in the SAR image that allows the main watercourse channel to be extracted.
2. The backscatter image pixel values are compared to the watercourse pixel values to check for similarity and to extract the entire wetted area.
3. Two images acquired before and during the flood are used to monitor changes in backscattering so that only those pixels that significantly change their backscatter values compared to their baseline values (*i.e.,* those from the SAR image used as a benchmark), are considered in the map of the flood extent [32].

The methodology presented allows us to evaluate multi-temporal maps of the most significant flood events that affected the Basento River. More specifically, Fig. 4 shows the two flood maps for the December 2013 event and the map of flooded areas at an instant close to the flood peak of the March 2011 event (see Fig. 5).

3.7. FLORA-2D hydrodynamic two-dimensional model

The hydraulic model used to produce the event scenario maps for different return times is a two-dimensional model based on De Saint-Venant's equations suitable for simulating flood propagation even in flat and mouth areas with complex topography, *i.e.,* the FLORA-2D (FLOod and Roughness Analysis) model [21].

The FLORA-2D model considers the two horizontal components of motion while neglecting the vertical components, which are generally small in floods of flat areas, and is based on the so-called De Saint-Venant's shallow water equations. The FLORA-2D model can simulate the time as well as space variability of resistance to motion because it allows the calculation of Manning's roughness coefficient n by distinguishing between rigid and flexible vegetation and, in the latter case, between total and partial submergence. In fact, this coefficient depends not only on the characteristics of vegetation cover, but also on the height of the water that hits the plant, which, in turn, varies over time during the flood event. This physical-process is of particular interest in the selected case study where there is a wide vegetated and agricultural area.

Among the factors affecting the extent of floodable areas and the water depth reached during a flood event, there is the resistance to motion offered by the vegetation in watercourses and floodplain areas.

Although the resistance offered by plants during a flood varies depending on the height reached by the water, hydraulic simulation models generally consider the value of the resistance to motion to be constant over time and expressed as Manning's (n), Chezy's (C) or Darcy-Weisbach's (f) roughness coefficient. The most suitable values chosen to characterise these coefficients involve a margin of uncertainty. This explains the choice of a hydraulic model capable of calculating both the space and time variation of the coefficient of resistance to motion offered by vegetation using the formulations proposed by Freeman et al. [33] and Petryk & Bosmajian [34] for herbaceous vegetation and trees, respectively.

Finally, previous studies have shown excellent results of the FLORA-2D model inherent to the assessment of flood scenarios in several applications [35] also in the Basilicata region (*e.g.,* Ref. [13]), though not directly concerning the mouth of the Basento River.

Fig. 4. Flooded areas derived from Cosmo SkyMed SAR images on a) December 2, 2013, b) December 3, 2013 and c) March 3, 2011.

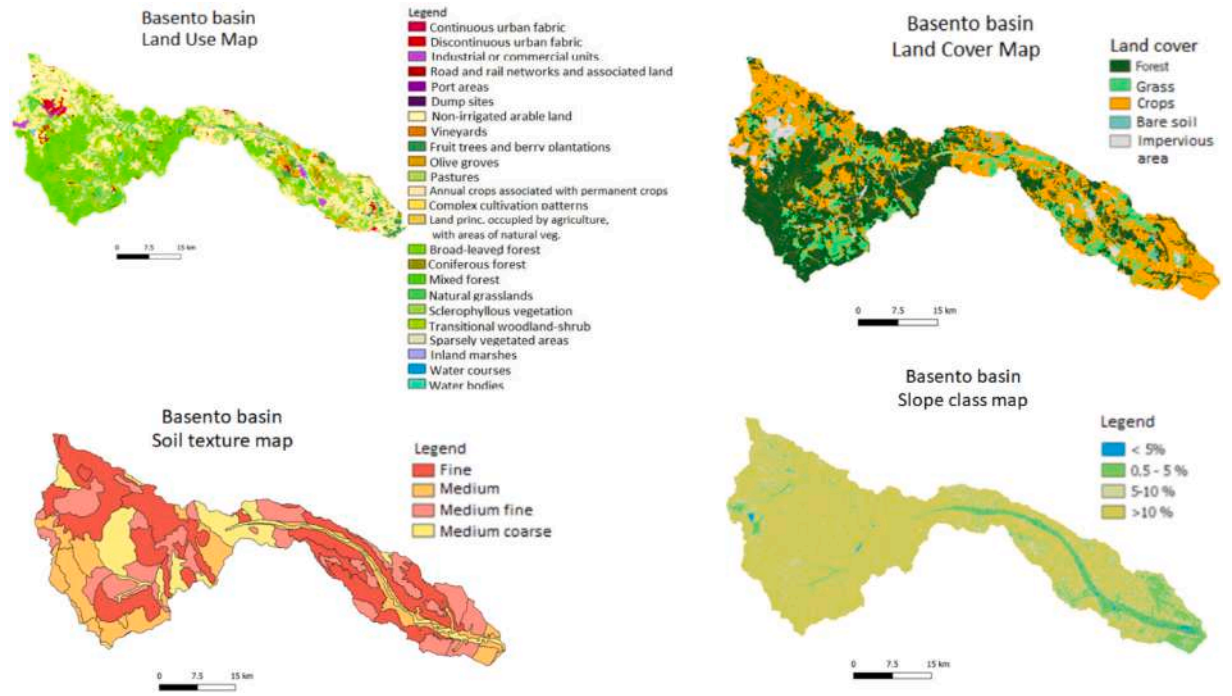

Fig. 5. Maps used to estimate outflow coefficient C and hydraulic parameters K_s, n, θ_c and β.

3.8. Calibration and validation of the FLORA-2D hydrodynamic two-dimensional model

The FLORA-2D hydrodynamic model was calibrated at the mouth of the Basento basin based on the Basento River flood event of 2–3 December 2013. The maps of the flooded areas were derived from the two SAR images, acquired during the event, whereas validation was carried out on the March 3, 2011 event, for which only one SAR image is available during the flood event, acquired after the flow rate had peaked. The validation of the model is a subsequent verification of the calibration and is necessary to assess the effectiveness of the modelling under different operating conditions.

The performance of each model simulation was analysed in terms of flood extent by comparing it (pixel by pixel) with the flood maps extracted by SAR image time series. However, the presence of dense vegetation emerging from water produced high radar return that decreased the contrast between flooded and non-flooded areas in SAR images and, therefore the water was hardly detected.

The highest amount of uncertainty among the hydraulic model parameters is soil roughness, as indicated by several studies such as Albano et al. [35] or Scaprino et al. (2018), particularly for 2D hydraulic models because it can affect the extent and timing of the flood and it can also generate localised processes.

Therefore, the calibration of the model was performed from six different values of Manning's coefficients (as in Ref. [13]) for the main watercourse channel and the floodplain. Plausible values of Manning's coefficient ranged between 0.04 and 0.1: a low roughness coefficient of 0.04 represents a fairly clean channel, while a high roughness coefficient of 0.1 represents a channel with very dense vegetation. The values of Manning's roughness coefficients used were as follows: (i) 0.04, (ii) 0.08 or (iii) 0.1 for channel and floodplain, (iv) 0.033 for the channel and 0.06 for floodplain areas (typical of a wet season), (v) 0.025 for the channel and 0.04 for the floodplain areas (typical of a dry season) and, finally, (vi) values that are spatially variable, parameterised based on different land-use categories as in Albano et al. [35].

The first stage of the calibration procedure is based on maps of the flood extent derived from a time series of SAR images (resampled to the same resolution as the hydraulic model, *i.e.,* 5 m, to avoid unbearable computation times). The FLORA-2D hydraulic model is incapable of simulating water infiltration into the soil. Therefore, to ensure consistency of calibration and validation, pixels in the SAR- and DEM-derived flood maps and hydraulic models were labelled as flooded where the water depth exceeded 0.1 m [13]. Comparing maps characterised by a series of Manning's coefficients (obtained from simulations with the FLORA-2D model) and SAR-derived maps over the same time interval generates a matrix, called a contingency table [36], of four possible results. Taking the SAR-derived maps as the true data reference, there are two conditions to correctly identify the flooded area (true positives, *TP* and true negatives, *TN*) and two ways to identify errors of underestimation or overestimation of the flood extent (false positives, *FP* or false negatives, *FN*) and their sum is called *SE*: *TP,* namely the total number of expected positive pixels that actually turn out to be positive (*i.e.,* flooded); *FP* is the number of expected positive pixels that turn out to be negative (*i.e.,* not-flooded); *TN* is the number of expected negative pixels that turn out to be negative; *FN* is the number of expected negative pixels that turn out to be positive.

In particular, the performance metrics used here were called sensitivity (Eqn 3) and specificity (Eqn 4) and were evaluated by the following equation:

$$\text{Sensitivity} = \frac{TP}{TP + FN} \tag{3}$$

$$\text{Specificity} = \frac{TN}{FP + TN} \tag{4}$$

Moreover, an additional metric, accuracy (Eqn 5), that represents the proportion of correctly classified pixels, was calculated using the following formula:

$$\text{Accuracy} = \frac{TP + TN}{TP + FP + TN + FN} \tag{5}$$

4. Results

4.1. Results of the AD2 inflow-outflow model calibration for the Basento basin

To calibrate the parameter values for the bucket equations of the AD2 model and its application to the Basento basin, it was initially necessary to estimate the range within which the model parameter values plausibly fall, from detailed information about the characteristics of the soils forming part of the catchment area, and in particular: soil cover, use and texture.

First, to estimate outflow coefficient C and hydraulic parameters K_s, n, θ_c, β, the soil cover and texture characteristics and the basin-specific slope classes are used. These maps are also available, at a scale of 1:5000, on the Geoportal of the Basilicata Region (http://rsdi.regione.basilicata.it/) or can be generated from these data (*e.g.,* slope classes defined from the DTM with 5 m resolution available on RSDI).

The initial estimate of the outflow coefficient C, with reference to the method proposed by Liu [37], is a function of soil use, soil class and slope while the calculation of hydraulic parameters Ks, n, θc and β requires the exclusive knowledge of the soil particle size classes.

Once the physically plausible variation ranges of coefficients C, S_c, $S_{\max}$, c, K_s, β, α_s and α_{sub} are assumed (see Table 2), the initial condition data are introduced into the model, namely surface moisture condition S_{ini}, initial surface volume Ws_{ini}, initial sub-surface volume $Wsub_{ini}$ and baseline flow rate Q_b.

The precipitation data from the historical event of December 2013 (from November 30 p.m. to December 3 late pm) were used as input for the AD2 to perform model calibration. The average precipitation values over the basin area were evaluated using the Thiessen polygon method from point data taken from rain gauges (see Fig. 2). To apply the fitness function, model results were compared with the flow rate measured at the "Basento SS 106" closure section. The results are found in Table 2 and Fig. 6. During the December 2013 event, the water depth at the ridge was 7.58 m in the case of the observed flow rate and 7.20 m in the case of the reconstructed flow rate, with a difference of only 5 %.

4.2. Results of the AD2 inflow-outflow model validation in the Basento basin

To check the transferability of the AD2 model calibration parameters to the so-called "out-of-sample situations", that is, when applied to hydrological conditions that significantly differ from those which calibration referred to, the model was validated by an application to another event, *i.e.,* March 2011. Using the parameter values evaluated during calibration, results obtained for March 2011 are shown in Fig. 7.

During validation and calibration, the NSE value turns out to be close to 1 (0.91 and 0.86, respectively), demonstrating that the simulated flow rate value is very close to the observed one, as shown in the figures above. The ratio between estimated (*e.g.,* for 2013 event equal to 228.7 mln m^3) and observed volumes (*e.g.,* for 2013 event equal to 247.8 mln m^3) is also a measure of the model's performance as it provides a detail on the goodness and accuracy of the model in the simulation phase: a value very close to 1 indicates that the overall estimated volumes are very similar to those actually transited.

4.3. Results of the estimation of flood hydrographs for event scenarios with return times of 30, 200 and 500 Years in the Basento basin

To reconstruct the rainfall events with return times of 30, 200 and 500 years, a preliminary analysis was performed to investigate the reliability of a synthetic hyetograph to reproduce the occurred flood events. After identifying the pluviometric stations within the basin and determining the areas pertaining to each pluviometric station, for each weather station considered, the return time for the available rainfall heights was estimated. In order to assign the basin-wide return time, the return times were weighted by the areas of

Table 2
Variation range values of the AD2 model parameters in the search range of the genetic algorithm and optimal values after calibration for the December 2013 event.

id	Name	valmin	valmax	Description	Optimal Value
1	C	0.1	0.9	Surface run-off coefficient	0.547
2	S_c	1	30	Water content at field capacity (mm)	6.538
3	S_{max}	10	400	Soil storage capacity (mm)	52.316
4	c	0.01	0.05	Sub-surface flow velocity coefficient (l/h)	0.041
5	K_s	4	80	Permeability at saturation (mm/h)	9.969
6	c_{soil}	5	30	Exponent of pore distribution in the soil	27.622
7	α_s	0.3	0.03	Surface run-off recession constant (l/h)	0.031
8	α_{sub}	0.2	0.01	Sub-surface run-off recession constant (l/h)	0.042

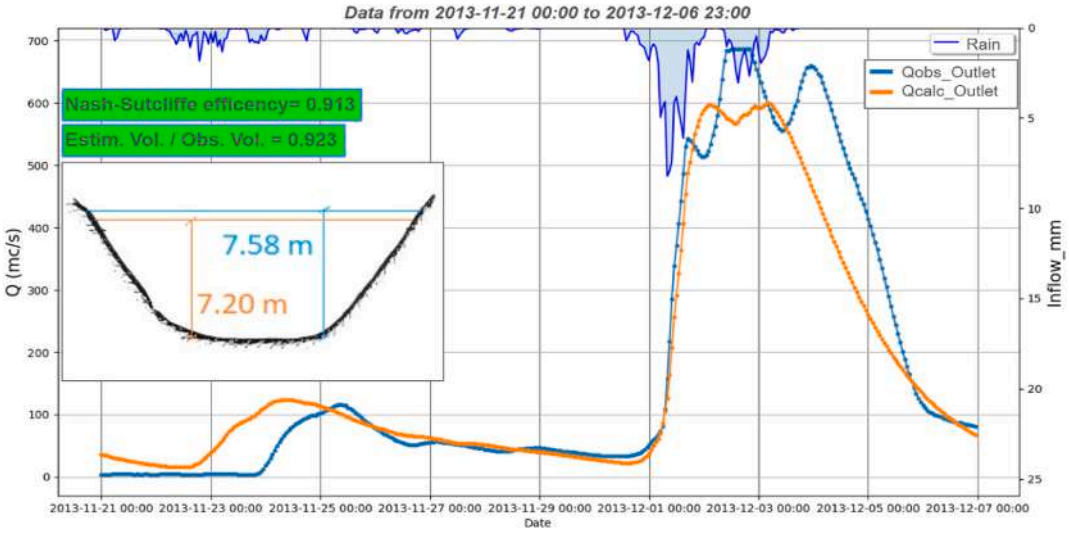

Fig. 6. Results of the estimation of the AD2 model flow rate for the December 2013 event compared with data observed at the "Basento SS 106" station.

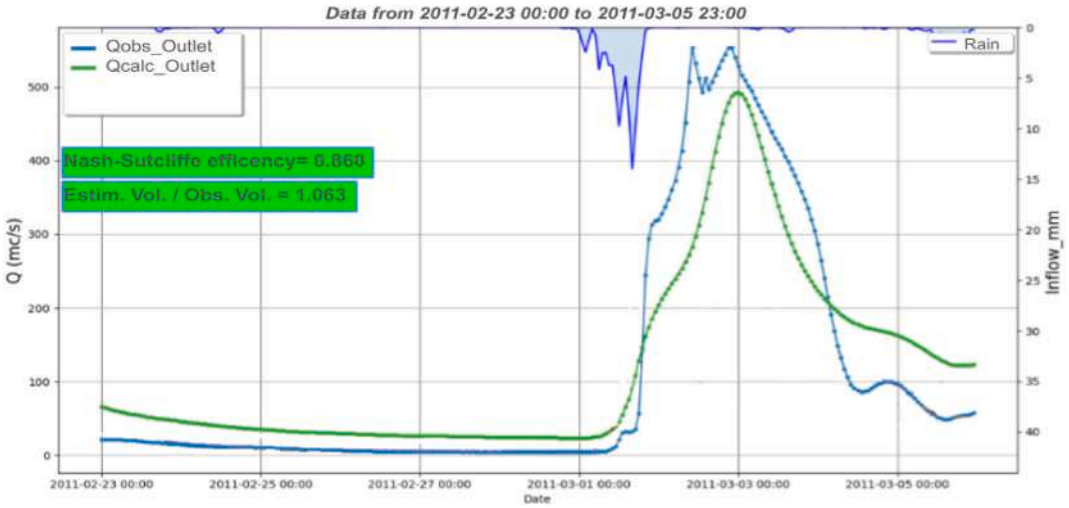

Fig. 7. Results of the estimation of the AD2 model flow rate for the March 2011 event compared with data observed at the "Basento SS 106" station.

the station within the basin. On average, the events of 2011 and 2013 are located at return time curves of 12 and 19 years respectively. The rainfall events of 2011 and 2013 were then reproduced in synthetic form using an alternating block hyetograph of the "Chicago" type with a sampling interval of 60 min and duration 2-times larger than the concentration time (Tc = 24 h). After selecting the rainfall duration, the design hyetograph was derived by adopting the symmetric Chicago approach, *i.e.,* with a value of rc = 0.5 (Fig. 8).

The synthetic hyetograph with a return time of 19 years, calculated for the December 2013 event, was the input for the AD2 model, using the parameters calibrated as described above for the 2011 flood event (Table 2). Fig. 9 shows the hydrograph simulated by the

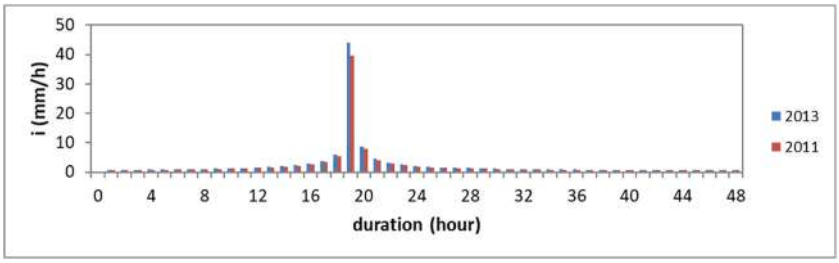

Fig. 8. Chicago hyetograph for the simulation of the March 2011 and December 2013 events.

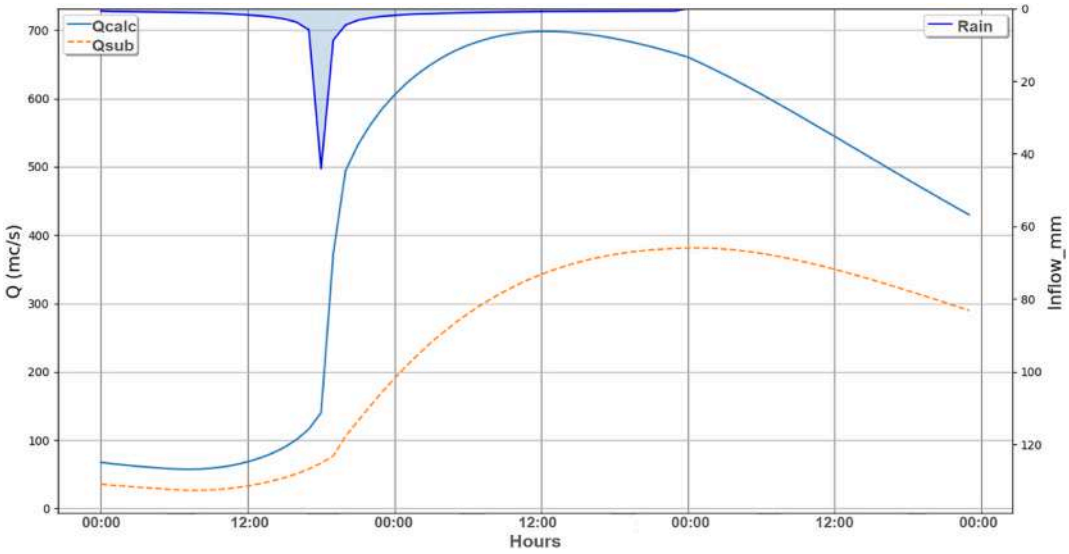

Fig. 9. Hydrograph simulated with the AD2 model using the design hyetograph with a return time of 19 years.

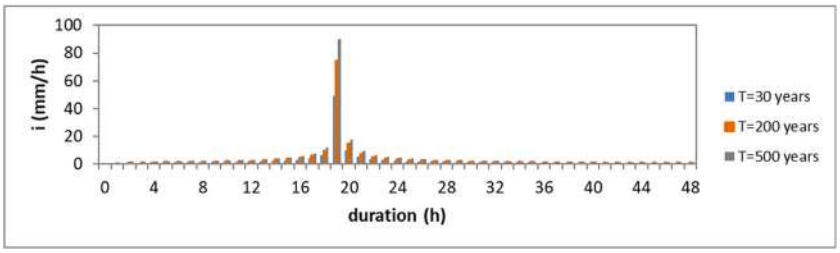

Fig. 10. - Chicago hyetograph estimated for the flood events with $T_R = 30$, 200 and 500 years.

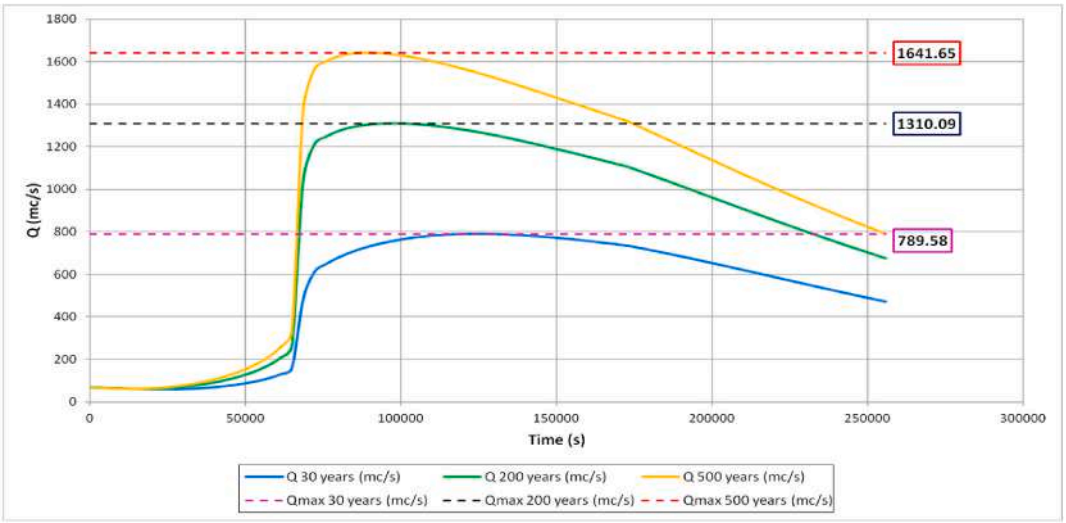

Fig. 11. AD2-simulated hydrographs for flood events with $T_R = 30$, 200 and 500 years.

AD2 model using the Chicago hyetograph as input, with a central peak for $T_R = 19$ years, which shows a maximum flow rate at the ridge of 700 m^3/s, very close to the observed value of 687 m^3/s.

The results of this comparison show that the application of synthetic hyetographs estimated for more extreme events than that of December 2013, *i.e.,* with high, hence less frequent, return times ($T_R = 30$, 200 and 500 years), applied as input to the appropriately calibrated AD2 model (see Section 3.4), can produce reliable flood hydrographs. Therefore, the DDFs curves with $T_R = 30$, 200 and 500

years were defined using the weighted average of parameters a and n of the stations under examination. The parameters "a" and "n" were obtained from the VAPI report and subsequent updates [18]. The growth factor used to define the rainfall height for a predefined return period was taken from the VAPI report for the Basilicata region for homogeneous sub-zone A. The estimated parameters are: $a =$ 25.66 mm and $n = 0.26$. Therefore, Chicago hyetographs with $T_R = 30$, 200 and 500 years were defined in a similar manner as previously described (Fig. 10) and hydrographs were simulated with the AD2 model (Fig. 11). Results show that the peak discharge values, for $T_R = 30$, 200 and 500 years, were 789.58 m^3/s, 1310.09 m^3/s and 1641.65 m^3/s, respectively.

4.4. Results of the calibration of the FLORA-2D hydrodynamic model on historical events at the mouth of the Basento basin

As previously mentioned, the calibration of the FLORA-2D model was based on the 2–3 December 2013 event using six different Manning's roughness values for the main channel and surrounding areas. This process consists of a series of steps that allow the model to provide maps containing the wetted cells (*i.e.,* the flood extent) and the water depth. The first step was to generate the 6 different simulations based on the 6 different combinations of roughness values considered (0.04, 0.08, 0.1, 0.033 for the channel and 0.06 for the floodplain areas, 0.025 for the channel and 0.04 for the floodplain areas and roughness variable in space), then to compare these with the images provided by the SAR. Below are the maps generated with FLORA-2D for the various roughness values and in yellow the wetted areas extracted by SAR images (see Figs. 12 and 13).

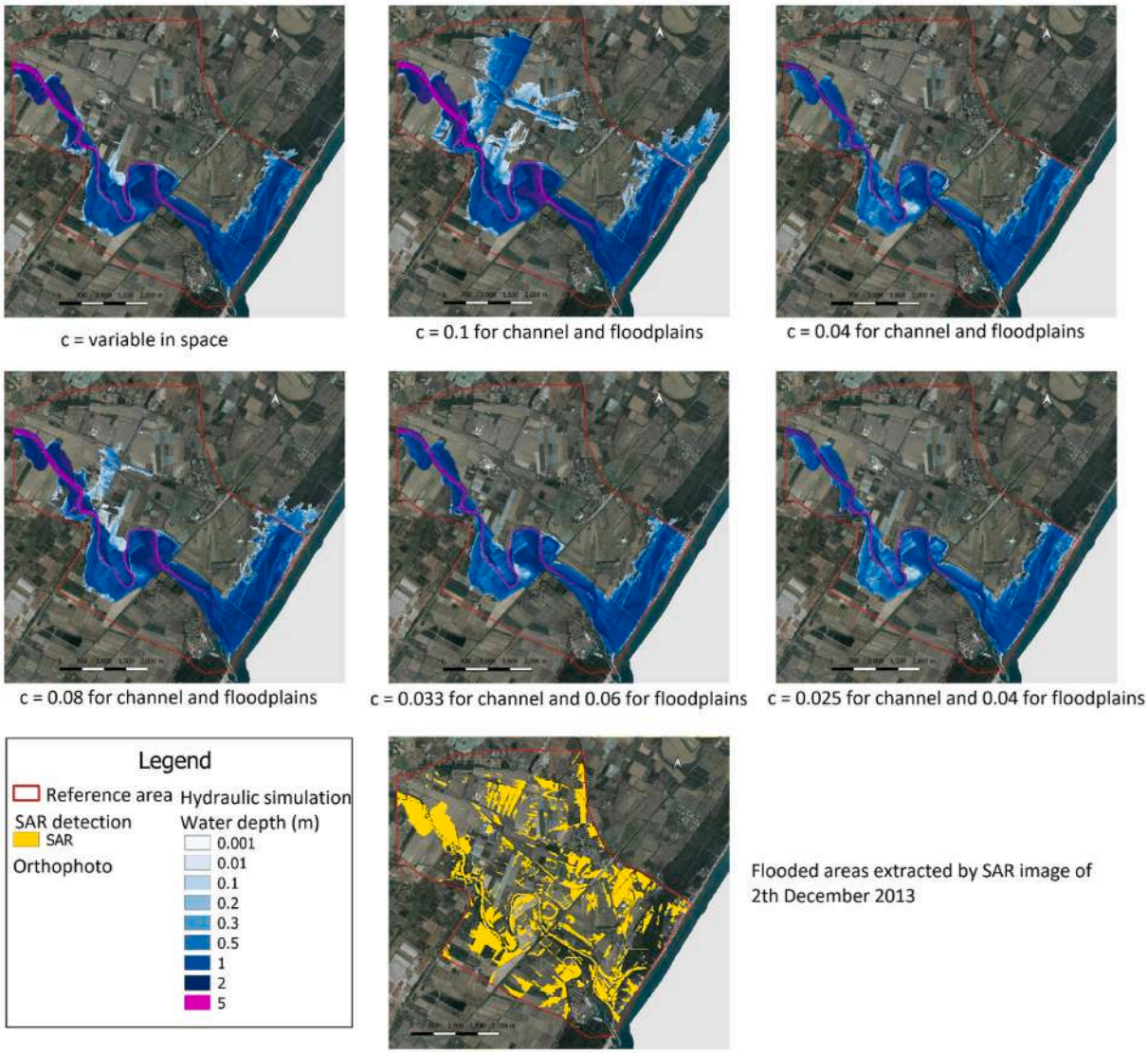

Fig. 12. Comparison of the six hydrodynamic simulations of the FLORA-2D model featuring different values of Manning's coefficient and the SAR-derived map for December 2, 2013.

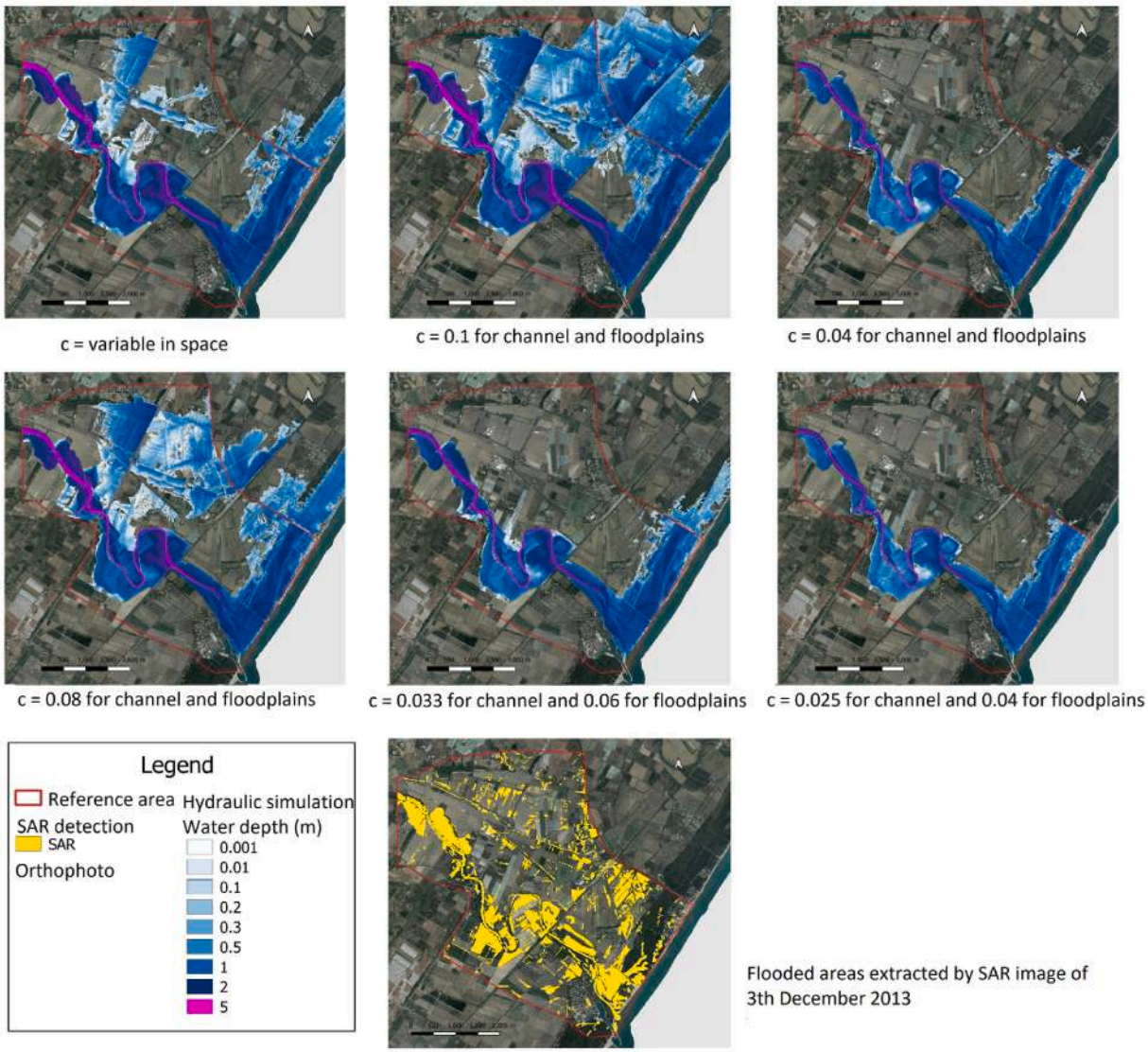

Fig. 13. Comparison of the six hydrodynamic simulations of the FLORA-2D model featuring different values of Manning's coefficient and the SAR-derived map for December 3, 2013.

Tables 3 and 4 show the results of the calibration performance metrics (Accuracy, Sensitivity, Specificity, SE) related to the comparison, in terms of flood extent, between hydraulic model simulation using different roughness parameters and the SAR flood area maps for 2 and December 3, 2013.

The results showed a good match between the SAR-derived and the FLORA-2D-simulated maps, demonstrating the reliability of the hydrodynamic model. In general, emphasis should be put on the fact that the December 2013 event was large in terms of rainfall intensity, so the uncertainty and sensitivity of the model were quite high along with the magnitude of the event.

Table 3
Results of the comparison between FLORA-2D simulations and SAR images for the December 2, 2013 event for different roughness values.

Results of the Raster Comparison between FLORA-2D simulations and SAR images for the December 2, 2013 event for different roughness values				
Roughness *c*	SE	Accuracy	Sensitivity	Specificity
variable in space	76.54 %	70.46 %	44.80 %	78.66 %
0.1 for the channel and floodplain areas	75.42 %	64.49 %	58.01 %	66.57 %
0.04 for the channel and floodplain areas	75.86 %	71.95 %	42.91 %	81.23 %
0.08 for the channel and floodplain areas	76.56 %	68.85 %	47.88 %	75.56 %
0.033 for the channel and 0.06 for the floodplain areas	76.09 %	71.49 %	43.48 %	80.43 %
0.025 for the channel and 0.04 for the floodplain areas	75.94 %	72.11 %	42.49 %	81.57 %

Table 4
Results of the comparison between FLORA-2D simulations and SAR images for the December 3, 2013 event for different roughness values.

Results of the Raster Comparison between FLORA-2D simulations and SAR images for the December 3, 2013 event for different roughness values				
Roughness *c*	SE	Accuracy	Sensitivity	Specificity
variable in space	61.60 %	69.58 %	68.54 %	69.86 %
0.1 for the channel and floodplain areas	67.83 %	56.04 %	83.70 %	48.47 %
0.04 for the channel and floodplain areas	60.89 %	77.37 %	55.84 %	83.27 %
0.08 for the channel and floodplain areas	65.08 %	61.51 %	77.91 %	57.01 %
0.033 for the channel and 0.06 for the floodplain areas	60.25 %	76.65 %	57.98 %	81.77 %
0.025 for the channel and 0.04 for the floodplain areas	60.72 %	77.62 %	55.64 %	83.64 %

The main analysis focuses on a critical evaluation of the simulations, both visually (analysing how and when the wave expands towards the surrounding areas) and numerically (with respect to the values obtained by comparing the results with SAR images), to identify which roughness values are best for the metrics considered. In this context, the simulations with Manning's roughness values of 0.08 $m^{-1/3}s$ for the channel and floodplain areas, 0.033 $m^{-1/3}s$ for the channel and 0.06 $m^{-1/3}s$ for the floodplain areas, and variable roughness were defined as the most suitable and true. The results seem quite similar and were the best among those considered. These roughness values were used to validate the model through the March 2011 event as reported in Section 4.5.

4.5. Validation of the FLORA-2D hydrodynamic model

As already mentioned, the validation of the hydrodynamic model was performed on the historical event of March 2011 using the simulations carried out with the three best Manning's roughness values considered to be better than the overall ones, namely 0.08 $m^{-1/3}s$ for the channel and floodplain areas, 0.033 $m^{-1/3}s$ for the channel and 0.06 $m^{-1/3}s$ for floodplain areas and variable roughness. The decision to reduce the number of simulations was based on the intention to define a single realistic and efficient roughness value, and exclude simulations that did not provide satisfactory results during calibration.

Proceeding in the same way as in the calibration phase and considering the same boundary conditions and domain, the maps in Fig. 14 were generated for the March 3, 2011 event with FLORA-2D for the three different roughness values that showed better performance in the calibration phase detailed in Sect. 4.4.

Table 5 shows the performance results of the hydrodynamic simulation model for the March 3, 2011 event in terms of the sum of overestimation and underestimation errors *SE*, Accuracy, Sensitivity and Specificity.

The simulation characterised by a roughness value that is variable in space, shows higher average values of Accuracy, Sensitivity and Specificity and, more importantly, results in a lower error value in terms of *SE* compared to other simulations.

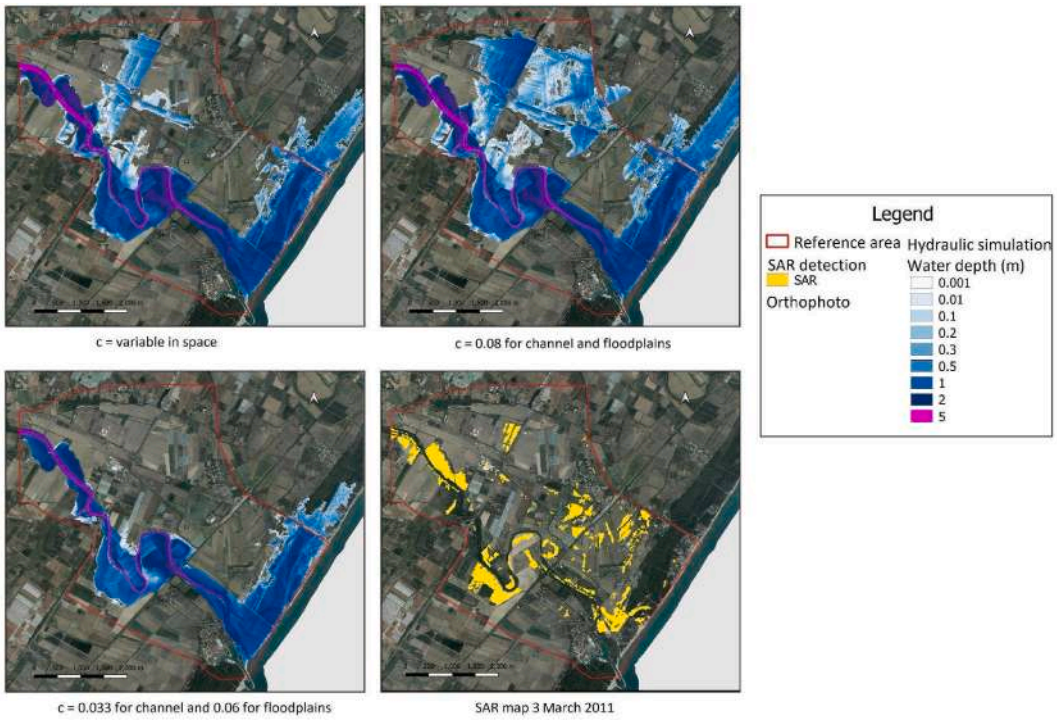

Fig. 14. Comparison of the three hydrodynamic simulations of the FLORA-2D model featuring different values of Manning's coefficient and the flood extent of SAR-derived map for March 3, 2011.

Table 5
Results of the comparison, in terms of flood extent, between FLORA-2D simulations and SAR images for the March 3, 2011 event for different roughness values.

Results of the Raster Comparison between FLORA-2D simulations and SAR images for the March 3, 2011 event for different roughness values				
Roughness *c*	SE	Accuracy	Sensitivity	Specificity
variable in space	57.06 %	68.39 %	75.19 %	67.75 %
0.08 for the channel and floodplain areas	60.63 %	57.03 %	84.99 %	54.38 %
0.033 for the channel and 0.06 for the floodplain areas	58.02 %	75.99 %	64.94 %	77.04 %

4.6. Discussion of the calibration and validation of the FLORA-2D hydrodynamic model

The calibration results in terms of true positives, as well as Sensitivity, on December 2, 2013, show better values than the false negatives. This not unexceptional result may be influenced by the considerable extension of the area under examination, which is far greater than the one affected on 3 December, with the probability of including flooded areas not due to the overflowing of the Basento (the physical process simulated by the hydrodynamic model), but due to local effects of the rain, thus causing the false negative value to increase. The same situation is evident also during validation of the March 2011 event that is less important in terms of maximum discharge and water volume than the Decembre 2013 flood event; however, the validation performances should be expected to slightly decrease in comparison to calibration.

Hence, better results were obtained for the simulations on 3 December in comparison with December 2, 2013, with the Sensitivity increasing significantly from 45 % to 70 %, while keeping quite stable Accuracy and Specificity values. Following the peak of the flood wave, the number of wetted cells detected in the SAR images corresponds more closely to those simulated by the FLORA-2D model, thus leading to a reduction in error, which in turn increases Sensitivity. Therefore, the SE value (sum of underestimation and overestimation errors) drops significantly compared to the previous simulation, from 75 % to 60 %, while the Sensitivity increases from around 44 % to between 55 and 83 %, depending on the Manning's roughness value used for the simulation.

It is important to note that SAR can have some limits in identifying the actual wetted areas in complex contexts such as those with high vegetation intensity, *e.g.,* pine forests or orchards and the presence of small depressions in the ground leading to the collection of rainwater. As can be noted in Fig. 15, the areas in which there are orchards or plantations are not identified by the SAR as flooded: in b) it is possible to observe areas with hydraulic discontinuities that are not due to a rise in ground level, as can be seen in c) and d). This situation leads not only to a decrease in the Sensitivity but also to an increase in the overall error.

Subsequently, we performed an analysis to estimate the elevation variability in an area where we found relevant discontinuities that were detected in the SAR-derived flooded areas. In this area (Fig. 15) the DEM doesn't shown an increase of elevation that could justify the hydraulic discontinuity (i.e. the separation between flooded and no flooded areas) highlighted in the SAR images.

Therefore, we calculated the average terrain elevation to obtain a threshold that could separate the dry and wetted parts of the surface. As can be seen from the DEM in Fig. 16, a natural border separates the floodplain area on the hydraulic right of the river from the rest of the territory: this is where the average elevation at which the cell was identified as wetted was assessed.

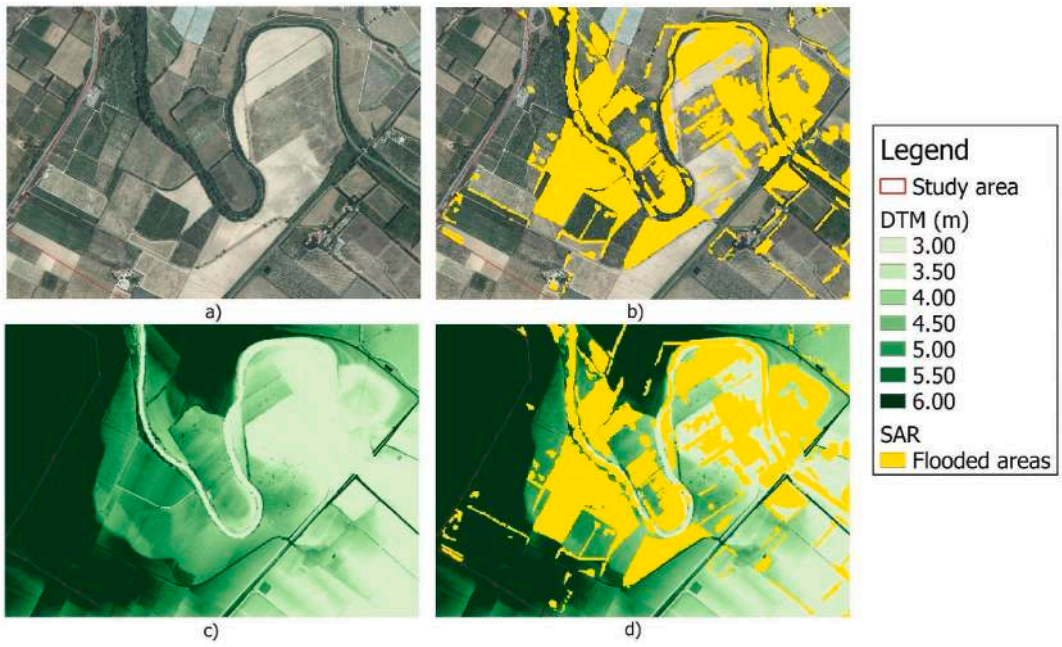

Fig. 15. SAR criticality identification: a) Orthophotos, b) Flooded areas detected by SAR, c) DTM, d) Flooded areas by SAR on DTM for the December 3, 2013 event.

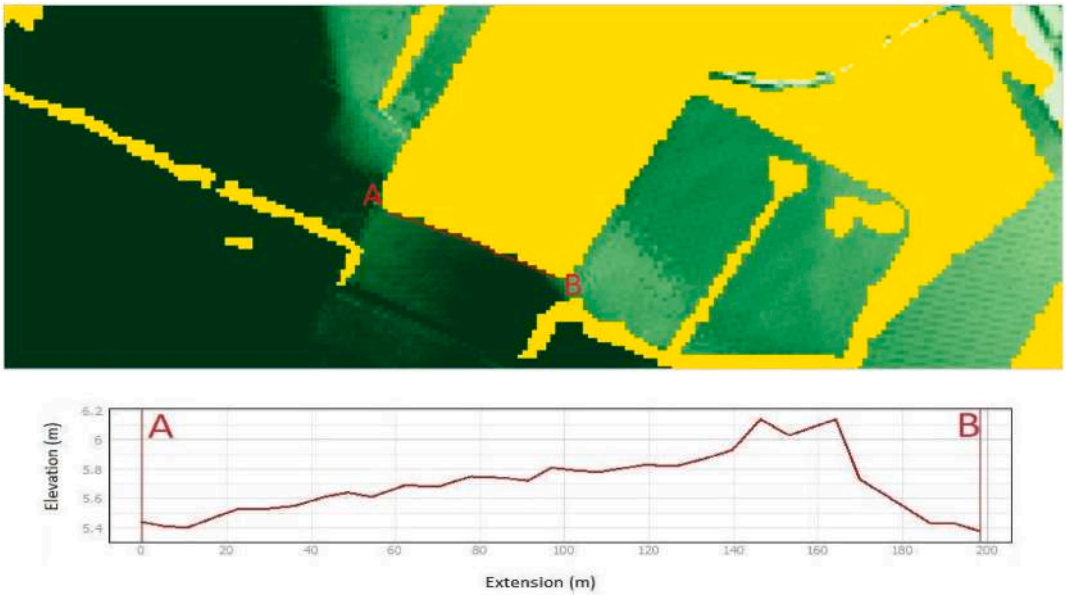

Fig. 16. Section for assessing the average elevation of the flooded terrain.

Moreover, tracing a section along the edge of the wetted area surveyed by the SAR (see Fig. 17), the average between the maximum value (6.22 m) and the minimum value (5.30 m) identified was 5.76 m, a threshold elevation that can be identified as the limit below which the area can be considered flooded.

The terrain profile shows that the area not detected by the SAR as wetted is located at an elevation of less than 5.76 m and is therefore desirable to be considered flooded. By extending this method, it is possible to identify, by way of example, the entire area on the left part of the image that can be considered flooded. By searching for all elevations below 5.76 m, it is possible to estimate the flood-prone areas below the estimated threshold (Fig. 18). The latter is visually compared with flooded areas identified by the SAR in Fig. 19.

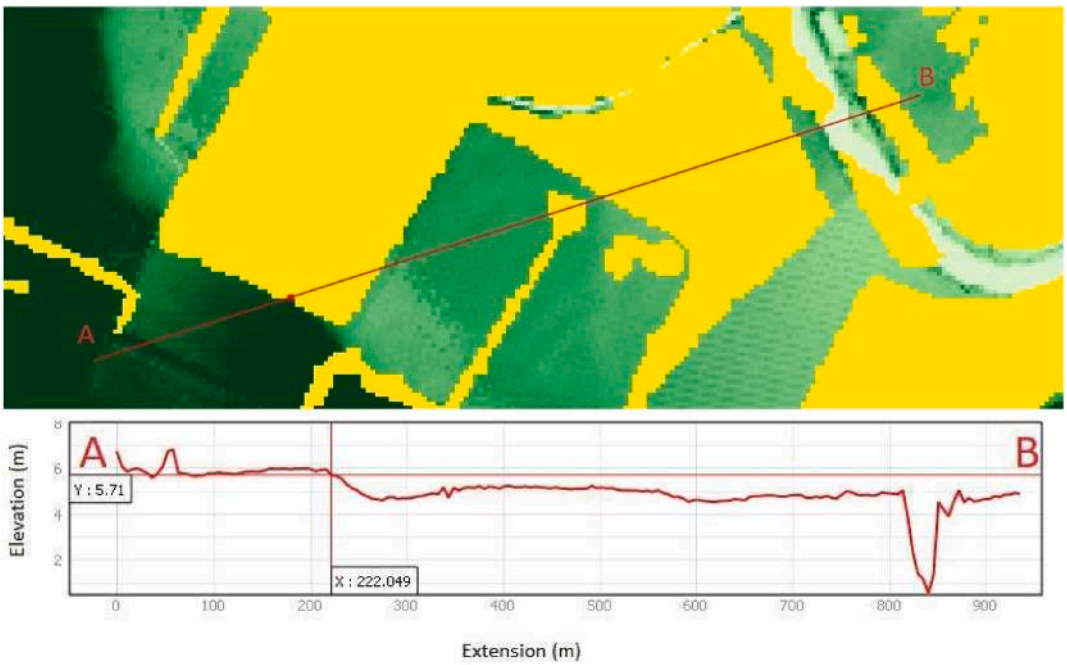

Fig. 17. Section for assessing the average terrain elevation.

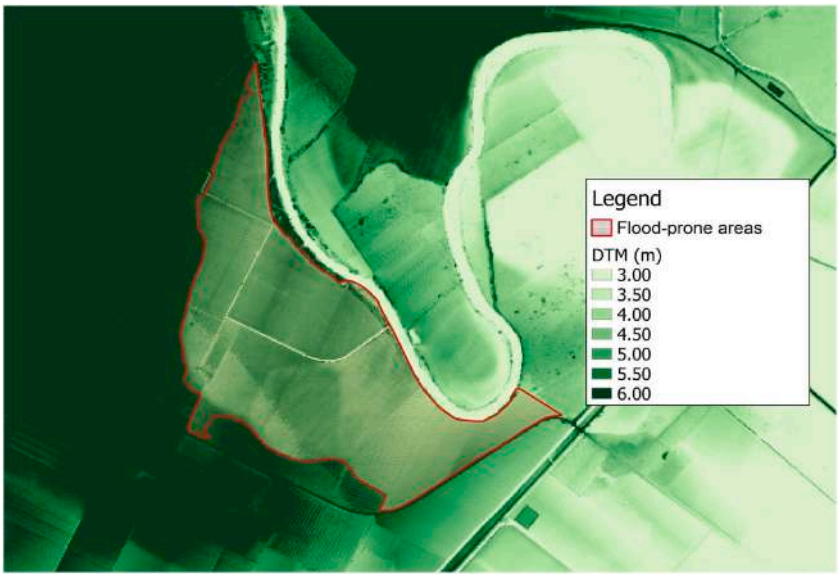

Fig. 18. Estimate of the flooded area below the calculated elevation threshold.

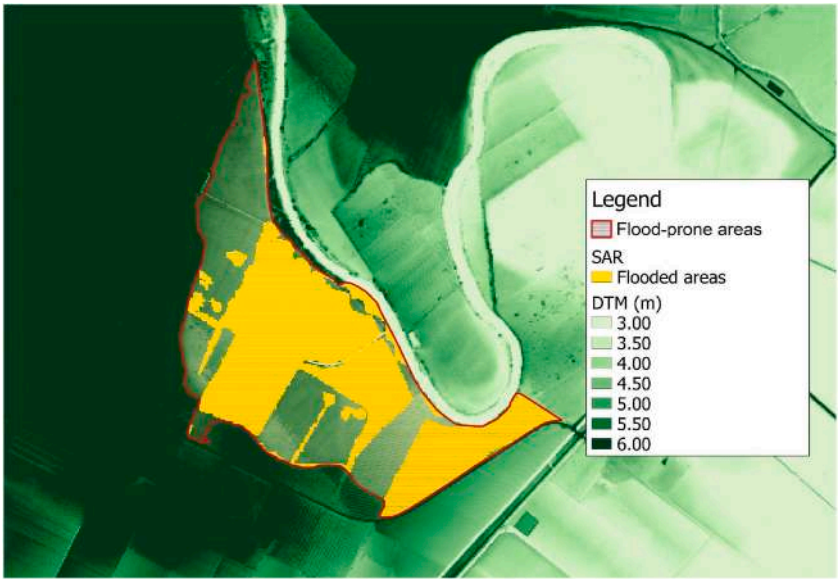

Fig. 19. Comparison of estimated flooded area and wetted area measured by the SAR.

Therefore, the value of accuracy that remains around 70 % of the FLORA-2D hydraulic model in comparison to SAR-derived flood maps is affected by the errors due to the inherent limits of SAR measurements. In fact, comparing the hydrodynamic model simulation with the flood-prone areas estimated previously based on the basis of the DEM, there is a relevant visual overlap, demonstrating that the accuracy of the model is remarkably high (see Fig. 20).

Finally, the presence of several depression areas that result in rainwater collection is highlighted in the following images of an agricultural field where the SAR-derived flood map is overlapped to an additional exemplificative FLORA-2D simulation (not considered in the calibration and validation phase of this study) where not only discharge but also rainfall rate was included as initial model conditions. It is evident that in this area the water stagnates due to soil saturation (see Fig. 21). However, rainfall rate was not used in the performed model simulation due to the large increase in computational time that could limit the operability of the modelling chain for flood early warning.

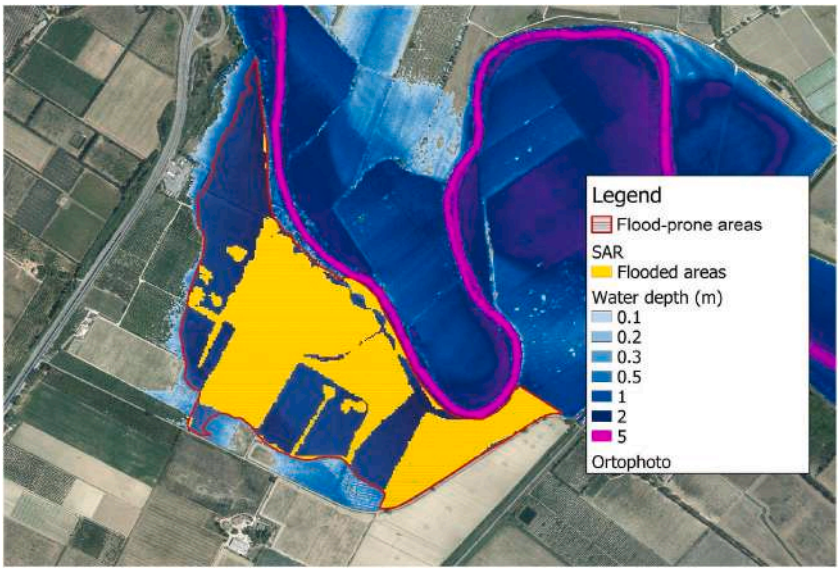

Fig. 20. Comparison between DEM-based flood prone areas, SAR-derived flood map, and FLORA-2D-generated hydraulic simulation.

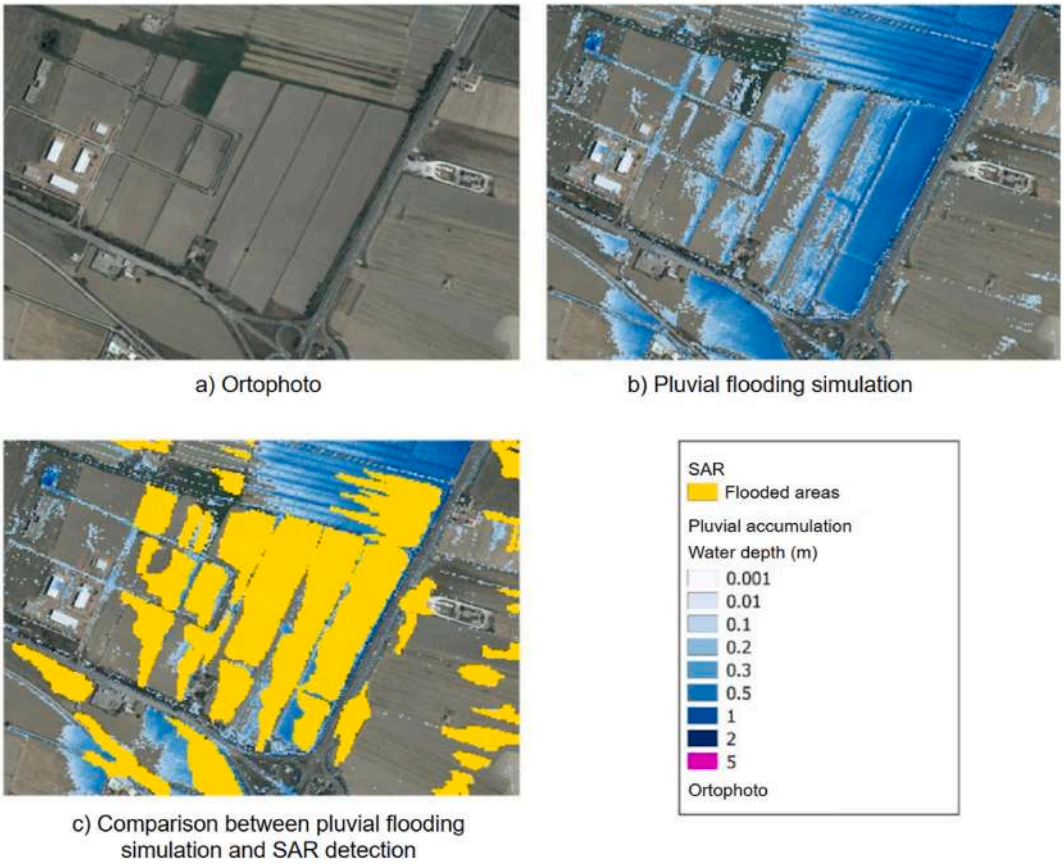

Fig. 21. Flooded areas due to soil saturation and water stagnation: a) Ortophoto, b) Pluvial flooding simulation and c) Comparison between pluvial flooding simulation and SAR detection.

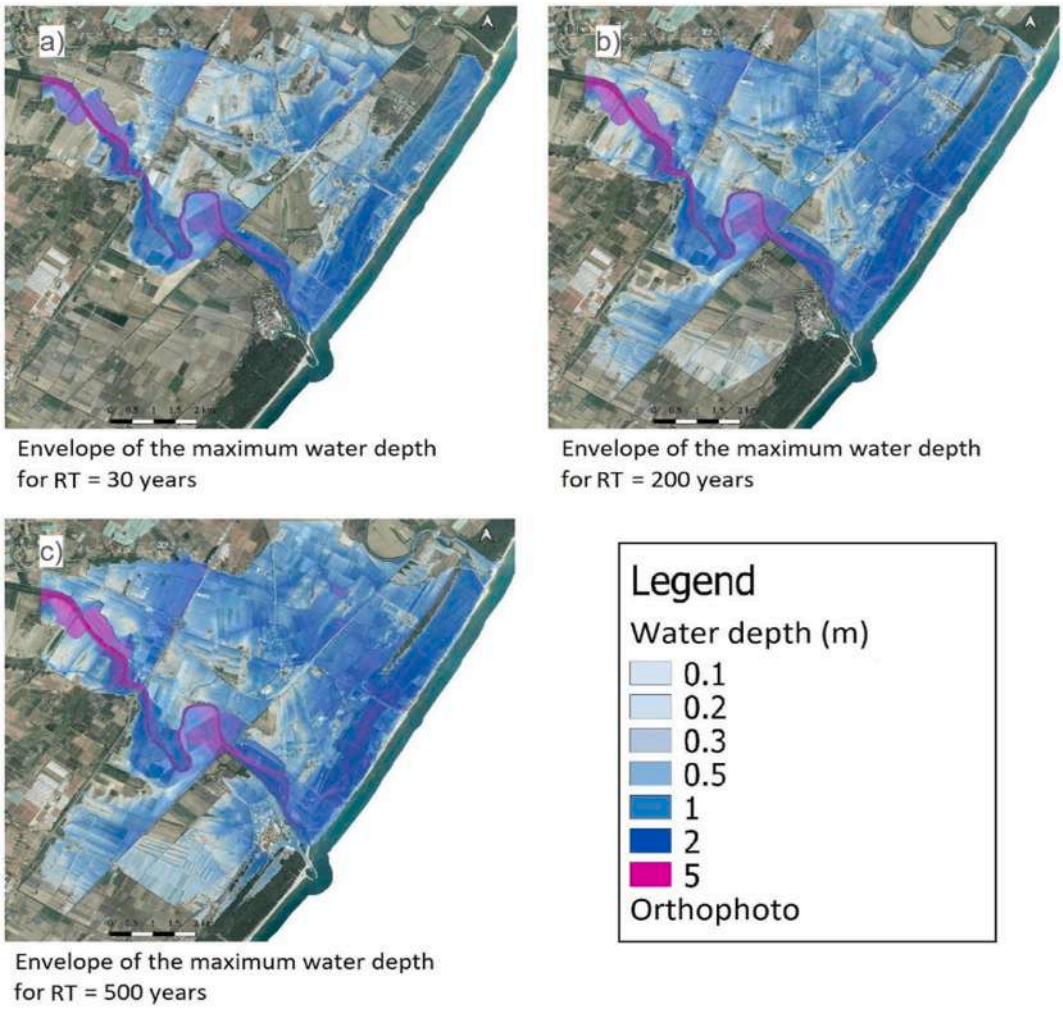

Fig. 22. Envelope of the maximum water depth for the return time scenarios of 30 (a), 200 (b) and 500 years (c).

4.7. Application of the FLORA-2D hydrodynamic model for event scenarios with return times of 30, 200 and 500 Years in the Basento basin

In view of what was described in the previous section, for event scenarios with return times of 30, 200 and 500 years, the simulations were carried out with the FLORA-2D hydrodynamic model using a Manning's roughness value that is variable in space. The hydrographs generated with the AD2 model for events with $T_R = 30$, 200 and 500 years, described in Section 4.3, were used for the three simulations.

Figure 22 showed the envelope of the maximum water depth for scenarios with return times of 30, 200 and 500 years: the extent of the areas affected by the flooding was 20.62, 31.87 and 36.35 km^2 for the scenarios with T_R of 30, 200 and 500 years, respectively.

5. Conclusions

In conclusion, it is safe to say that hydrodynamic modelling plays a decisive role in flood forecasting. In recent years, the need for a predictive system capable of providing hazard scenarios due to rainfall events that are becoming increasingly extreme and producing ever greater damage both to the territory and to people's lives, has become stronger than ever. The availability of model calibration methods is therefore of paramount importance to optimise the use of models and obtain timely and accurate results. In the regional and national context, these maps serve as a tool for flood early warning, to comply with the flood risk zoning requirements of the EU flood directive (EU 2006), and can be used more generally in the public sector of natural hazard communication to enhance risk awareness among the citizen. Indeed, the use of these models to realise hazard and hydraulic risk maps can support the evaluation of insurance policies, the planning of mitigation interventions and definition of priorities, the establishment of maintenance plans for riverbeds and territorial defence infrastructure, the choice and management of emergency or civil protection strategies, and the promotion of life-saving behaviours by citizens and stakeholders in case of a flood [38]. In addition, these models make it possible to assess the evolution of a flood in terms of space and time to provide civil protection operators with, for example, tools to assess which areas can be accessed

first and which roads should be restored in the short term. Locating where water stagnates allows the identification of areas where water retreat must be artificially accelerated through pumping [13].

The calibration of the AD2 hydrological model and subsequent validation using a genetic algorithm based on data recorded during the historical events of December 2013 and March 2011 led to excellent results with NSE indices of 0.91 and 0.86, respectively.

The calibration and subsequent validation of the FLORA-2D hydraulic model was also based on the 2013 and 2011 events. Comparing the resulting maps with the SAR images yielded results with an accuracy close to 70 %.

Once the calibration of both the AD2 hydrological model and the FLORA-2D hydraulic model were completed, it was possible to simulate event scenarios with return times of 30, 200 and 500 years.

It demonstrates that we have proposed a practical workflow characterized by efficiency and flexibility with a sufficient degree of automatization in calibration phase. Moreover, the quality of the hazard maps produced is based on the appropriate way of generalisation of the proposed workflow and the degree to which heterogeneous data can be combined at the required scale. Indeed, the framework clearly lends itself to application in other regions.

The significance of the overall study lies not only in its technical contributions to flood hazard modeling but also in its potential applications in comprehensive flood risk assessment and management. The findings from this research can be integrated with socio-economic data and used to develop risk-informed strategies aimed to mitigate the impacts of flood events.

Future developments envisage the implementation of a cascade forecasting system with the assimilation of rainfall data and SAR images in near real-time (or whenever they become available). This would allow a continuous calibration of hydrological and hydrodynamic models and realise short-term forecasts that are effective in describing different types of flood events of varying magnitudes in terms of space and time.

CRediT authorship contribution statement

Raffaele Albano: Writing – review & editing, Writing – original draft, Supervision, Software, Methodology, Funding acquisition, Formal analysis, Data curation, Conceptualization. **Carmine Limongi:** Validation, Formal analysis, Data curation. **Silvano Fortunato Dal Sasso:** Writing – review & editing, Writing – original draft, Formal analysis, Data curation. **Leonardo Mancusi:** Validation, Software, Formal analysis, Data curation. **Jan Adamowski:** Writing – review & editing, Writing – original draft, Visualization, Validation.

Declaration of competing interest

The authors declare the following financial interests/personal relationships which may be considered as potential competing interests: Raffaele Albano reports financial support was provided by University of Basilicata. Raffaele Albano reports a relationship with University of Basilicata that includes: employment.

Data availability

Data will be made available on request.

Acknowledgement

This research is inserted in the ODESSA (On DEmand Services for Smart Agriculture) project (financed by the European Regional Development Fund Operational Programme 2014–2020).

References

[1] C. Galasso, M. Pregnolato, F. Parisi, A model taxonomy for flood fragility and vulnerability assessment of buildings, Int. J. Disaster Risk Reduc. 53 (1 February 2021) (2021) 101985.
[2] R. Gentile, C. Gemma, C. Galasso, L.T. Jenkins, V. Manandhar, E.Y. Mentese, E. Guragain, J. McCloskey, Scoring, selecting, and developing physical impact models for multi-hazard risk assessment, Int. J. Disaster Risk Reduc. 82 (November 2022) (2022) 103365.
[3] R. Albano, L. Mancusi, J. Adamowski, A. Cantisani, A. Sole, A GIS tool for mapping dam-break flood hazards in Italy, ISPRS Int. J. Geo-Inf. 8 (6) (2019) 250, https://doi.org/10.3390/ijgi8060250.
[4] C. Mesta, G. Cremen, C. Galasso, Quantifying the potential benefits of risk-mitigation strategies on future flood losses in Kathmandu Valley, Nepal, Nat. Hazards Earth Syst. Sci. 23 (2023) 711–731, https://doi.org/10.5194/nhess-23-711-2023.
[5] P. Costabile, F. Macchione, L. Natale, G. Petaccia, Flood mapping using LIDAR DEM. Limitations of the 1-D modeling highlighted by the 2-D approach, Nat. Hazards 77 (2015) 181–204.
[6] N.M. Bhuyian, A.J. Kalyanapu, F. Nardi, Approach to digital elevation model correction by improving channel conveyance, J. Hydrol. Eng. ASCE 2015 (20) (2015) 1–10.
[7] S. Saksena, Investigating the role of DEM resolution and accuracy on flood inundation mapping. In: world environmental and water resources congress 2015: floods, droughts, and ecosystems, in: Proceedings of the 2015 World Environmental and Water Resources Congress, 2015, pp. 2236–2243.
[8] S. Cohen, G.R. Brakenridge, A. Kettner, B. Bates, J. Nelson, R. McDonald, Y.-F. Huang, D. Munasinghe, J. Zhang, Estimating floodwater depths from flood inundation maps and topography, JAWRA J. Am. Water Resour. Assoc. 54 (2018) 847–858.
[9] S. Dey, S. Saksena, V. Merwade, Assessing the effect of different bathymetric models on hydraulic simulation of rivers in data sparse regions, J. Hydrol. 575 (2019) 838–851.
[10] G. Di Baldassarre, G. Schumann, P.D. Bates, A technique for the calibration of hydraulic models using uncertain satellite observations of flood extent, J. Hydrol. 367 (2009) 276–282.
[11] G. Schumann, P. Matgen, L. Hoffmann, R. Hostache, F. Pappenberger, L. Pfister, Deriving distributed roughness values from satellite radar data for flood inundation modelling, J. Hydrol. 344 (2007) 96–111.

[12] S. Manfreda, L. Mita, F. Dal Sasso, C. Samela, S. Mancusi, Exploiting the use of physical information for the calibration of a lumped hydrological model, Hydrol. Process. 32 (10) (2018).
[13] S. Scarpino, R. Albano, A. Cantisani, L. Mancusi, A. Sole, G. Milillo, Multitemporal SAR data and 2D hydrodynamic model flood scenario dynamics assessment, ISPRS Int. J. Geo-Inf. 7 (3) (2018) 105.
[14] CEMS;https://emergency.copernicus.eu/.
[15] G. Ruiz-Pérez, J. Koch, S. Manfreda, K. Caylor, F. Francés, Calibration of a parsimonious distributed ecohydrological daily model in a data scarce basin using exclusively the spatio-temporal variation of NDVI, Hydrol. Earth Syst. Sci. Discuss. (2017) 1–33, https://doi.org/10.5194/hess-2016-573, submitted for publication.
[16] A. Sole, L. Giosa, R. Albano, A. Cantisani, The laser scan data as a key element in the hydraulic flood modelling in urban areas, International Archives of the Photogrammetry, Remote Sensing and Spatial Information Sciences - ISPRS Archives 40 (4W1) (2013) 65–70.
[17] P.D. Bates, Remote sensing and flood inundation modelling, Hydrol. Process. 18 (2004) 2593–2597, https://doi.org/10.1002/hyp.5649.
[18] S. Manfreda, S. Aurelia, G. De Costanzo, Le Precipitazioni Estreme in Basilicata, Universosud, 2015, p. 146 (ISBN: 978-88-99432-03-4).
[19] M. Bancheri, R. Rigon, S. Manfreda, The GEOframe-NewAge modelling system applied in a data scarce environ-ment, Water 12 (2019) 86, https://doi.org/10.3390/w12010086.
[20] B. Boots, Spatial tessellations, in: P. Longley, M.F. Goodchild, D.J. Maguire, D.W. und Rhind (Eds.), Geographical Information Systems, John Wiley & Sons, New York, etc, 1999.
[21] A. Cantisani, L. Giosa, L. Mancusi, A. Sole, FLORA-2D: a new model to simulate the inundation in areas covered by flexible and rigid vegetation, Int J Eng Innov Technol 3 (8) (2014) 179–186.
[22] J. Teng, A.J. Jakeman, J. Vaze, B.F.W. Croke, D. Dutta, S. Kim, Flood inundation modelling: a review of methods, recent advances and uncertainty analysis, Environ. Model. Software 90 (2017) 201–216, https://doi.org/10.1016/j.envsoft.2017.01.006. ISSN 13648152.
[23] J.E. Nash, J.V. Sutcliffe, River flow forecasting through conceptual models part I-A discussion of principles, J. Hydrol. 10 (3) (1970) 282–290.
[24] G. Ippolito, Appunti di Costruzioni Idrauliche, Liguori Editore, 1995.
[25] M. Fiorentino, S. Manfreda, La Stima dei Volumi di Piena dell' Adige a Trento con riferimento al rischio di Inondazione, vol. 2, 2004, pp. 115–122. ISBN 88-7740-382-9, Editoriale Bios.
[26] S. Manabe, Climate and the ocean circulation: 1. atmospheric circulation and the hydrology of the earths surface, Mon. Weather, Rev. 97 (11) (1969) 739–774.
[27] D. Koutsoyiannis, D. Kozonis, A. Manetas, A mathematical framework for studying rainfall intensity-duration-frequency relationships, J. Hydrol. 206 (1998) 118–135.
[28] P. Claps, M. Fiorentino, Rapporto di sintesi sulla valutazione delle piene, 1999.
[29] PGRA—Italian Flood Risk Management Plan,Appennino Meridionale District. Available online: https://www.distrettoappenninomeridionale.it/index.php/pdg-alluvioni-menu.
[30] L. Pulvirenti, N. Pierdicca, G. Boni, M. Fiorini, R. Rudari, Flood damage assessment through multitemporal COSMO-SkyMed data and hydrodynamic models: the Albania 2010 case study, IEEE J. Sel. Top. Appl. Earth Obs. Remote Sens. 2014 7 (2014) 2848–2855, https://doi.org/10.1109/JSTARS.2014.2328012.
[31] N. Pierdicca, L. Pulvirenti, M. Chini, L. Guerriero, L. Candela, Observing floods from space: experience gained from COSMO-SkyMed observations, Acta Astronaut. 84 (2013) 122–133, https://doi.org/10.1016/j.actaastro.2012.10.034.
[32] L. Giustarini, R. Hostache, P. Matgen, G.J. Schumann, P.D. Bates, D.C.A. Mason, Change detection approach to flood mapping in urban areas using TerraSAR-X, IEEE Trans. Geosci. Remote Sens. 51 (2013) 2417–2430, https://doi.org/10.1109/TGRS.2012.2210901.
[33] G.E. Freeman, W. Rahmeyer, R.R. Copeland, Determination of Resistance Due to Shrubs and Woody Vegetation, U.S. Army Engineer Research and Development Center, Vicksburg, MS, 2000. Technical Report ERDC/CHL TR-00-25.
[34] S. Petryk, G.B. Bosmajian, Analysis of flow through vegetation, in: Journal of the Hydraulics Division, vol. 101, ASCE, 1975, pp. 871–884, 7.
[35] R. Albano, A. Sole, J. Adamowski, A. Perrone, A. Inam, Using FloodRisk GIS freeware for uncertainty analysis of direct economic flood damages in Italy, Int. J. Appl. Earth Obs. Geoinf. 73 (2018) 220–229.
[36] N.M. Notarangelo, K. Hirano, R. Albano, A. Sole, Transfer learning with convolutional neural networks for rainfall detection in single images, Water 13 (5) (2021) 588, https://doi.org/10.3390/w13050588.
[37] Y. Liu, GIS-based spatially distributed hydrological modeling of the Barebeek catchment, in: MSc. Dissertation Water Resources Engineering, Free University Brussels, Brussels, Belgium, 1999, p. 86.
[38] H.B. Hamzah, Roadmap toward Effective Flood Hazard Mapping in Malaysia, 2005.
[39] REGIONE BASILICATA, Dipartimento Infrastrutture, OO.PP e Mobilità Ufficio Protezione Civile, Report evento marzo 2011 - Eventi pluviometrici del 01/03/2011, pp.2-3, 2011.
[40] REGIONE BASILICATA, Dipartimento Infrastrutture, OO.PP e Mobilità Ufficio Protezione Civile, Report evento dicembre 2013 - Eventi metereologici eccezionali dei giorni 1,2 e 3 Dicembre 2013 nel territorio della Regiona Basilicata, pp.2-5 (2013).